The adaptor protein Ste50 directly modulates yeast MAPK signaling specificity through differential connections of its RA domain

Nusrat Sharmeen[a], Traian Sulea[b,c], Malcolm Whiteway[d,*], and Cunle Wu[a,b,*]
[a]Division of Experimental Medicine, Department of Medicine, McGill University, Montreal, QC H4A 3J1, Canada; [b]Human Health Therapeutics Research Centre, National Research Council Canada, Montreal, QC H4P 2R2, Canada; [c]Institute of Parasitology, McGill University, Sainte-Anne-de-Bellevue, H9X 3V9 QC, Canada; [d]Department of Biology, Concordia University, Montreal, QC H4B 1R6, Canada

ABSTRACT **Discriminating among diverse environmental stimuli is critical for organisms to ensure their proper development, homeostasis, and survival. *Saccharomyces cerevisiae* regulates mating, osmoregulation, and filamentous growth using three different MAPK signaling pathways that share common components and therefore must ensure specificity. The adaptor protein Ste50 activates Ste11p, the MAP3K of all three modules. Its Ras association (RA) domain acts in both hyperosmolar and filamentous growth pathways, but its connection to the mating pathway is unknown. Genetically probing the domain, we found mutants that specifically disrupted mating or HOG-signaling pathways or both. Structurally these residues clustered on the RA domain, forming distinct surfaces with a propensity for protein–protein interactions. GFP fusions of wild-type (WT) and mutant Ste50p show that WT is localized to the shmoo structure and accumulates at the growing shmoo tip. The specifically pheromone response–defective mutants are severely impaired in shmoo formation and fail to localize ste50p, suggesting a failure of association and function of Ste50 mutants in the pheromone-signaling complex. Our results suggest that yeast cells can use differential protein interactions with the Ste50p RA domain to provide specificity of signaling during MAPK pathway activation.**

Monitoring Editor
Daniel J. Lew
Duke University

Received: Nov 19, 2018
Revised: Jan 7, 2019
Accepted: Jan 9, 2019

INTRODUCTION

The development and survival of organisms depends on their ability to receive environmental stimuli and transduce them through signaling pathways to elicit specific responses that control cellular processes. This is accomplished by numerous modular signaling pathways (Mayer, 2015). Many signaling pathways share common component(s). A fundamental question in the field of signal transduction is how the myriads of inputs are sensed, integrated, and transduced accurately so that each elicits a specific and proper biological response.

A well-studied example of component overlap is found in the yeast *Saccharomyces cerevisiae*. Shared components are found in three major mitogen-activated protein kinase (MAPK) signaling pathways—the mating pheromone response pathway, which controls a developmental transition in response to pheromone, the high-osmolarity glycerol (HOG) pathway, which maintains homeostasis in response to environmental stress, and the pseudohyphal growth pathway, which controls cellular morphology in response to nutrient signals (Herskowitz, 1995). One of the shared components of these pathways, MAP3K Ste11, is part of the basic MAPK module consisting of MAP3K, MAP2K, and MAPK; this module is highly conserved among eukaryotes (Figure 1). MAP3K Ste11, which is located at the top of these MAPK modules, serves as a critical point of regulation in MAPK signaling (Craig *et al.*, 2008). For normal function, Ste11 kinase must interact with the Ste50

This article was published online ahead of print in MBoC in Press (http://www.molbiolcell.org/cgi/doi/10.1091/mbc.E18-11-0708) on January 16, 2019.

Author contributions: C.W., M.W., and N.S. conceptualized the project; N.S., C.W., and M.W. developed the methodology; N.S. did the investigation; N.S. performed formal analysis; T.S. carried out structural bioinformatics studies; N.S. wrote the original draft, and T.S. wrote the Figure 5 section; N.S., M.W., C.W., and T.S. edited the manuscript.

*Address correspondence to: Malcolm Whiteway (Malcolm.whiteway@concordia.ca) and Cunle Wu (Cunle.Wu@cnrc-nrc.gc.ca).

Abbreviations used: HOG, high-osmolarity glycerol; IVR, in vivo recombination; PPI, protein–protein interaction; RA, Ras association; SAM, sterile alpha motif.

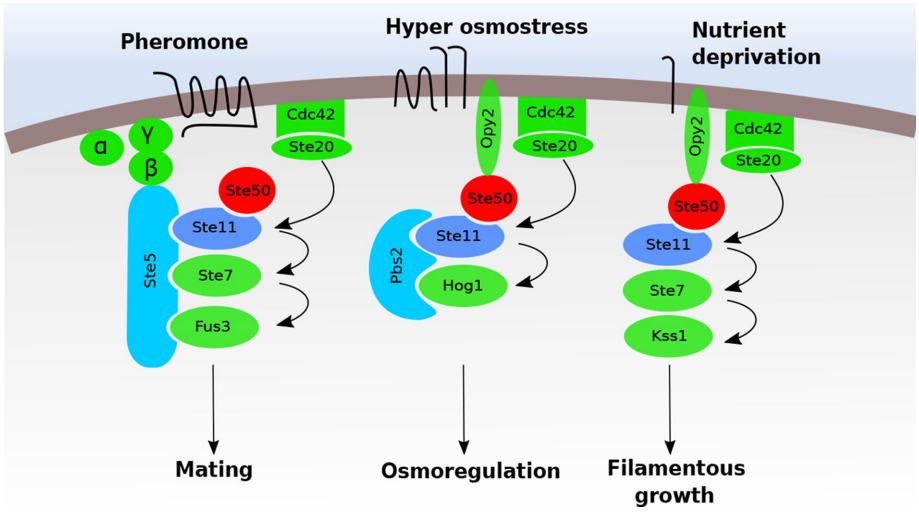

FIGURE 1: MAPK pathways with shared components in *Saccharomyces cerevisiae*. The pheromone, osmostress and nutrient deprivation are the three MAPK pathways that regulate mating, osmostress, and filamentous growth. All three pathways share the MAP3K Ste11 and the adaptor protein Ste50 that interacts with Ste11p (Gustin *et al.*, 1998; Posas *et al.*, 1998; Wu *et al.*, 1999; Jansen *et al.*, 2001; O'Rourke *et al.*, 2002).

adaptor protein, which is a small multidomain protein consisting of a conserved N-terminal SAM (sterile alpha motif) and a C-terminal RA (Ras association) domain connected by a linker region. Previous studies have established that the interaction of the Ste50 SAM domain with the SAM domain of Ste11 (MAP3K) is necessary for Ste11p function in all three pathways—pheromone response, hyperosmotic stress regulation, and pseudohyphal growth (Gustin *et al.*, 1998; Posas *et al.*, 1998; Wu *et al.*, 1999; Jansen *et al.*, 2001; O'Rourke *et al.*, 2002; see Figure 1). Studies have shown that costimulating individual yeast cells with pheromone and osmotic stress activates both pathways independently without interference, indicating sufficient insulation for pathway specificity (Patterson *et al.*, 2010).

A general theme of adaptor protein recruitment in a signaling pathway is amplification of signaling through contribution of additional docking sites for modular signaling (Pawson and Scott, 1997). Adaptors involved in specificity of signaling have been extensively documented (Songyang *et al.*, 1993; Stein *et al.*, 2003; Qamra and Hubbard, 2013), and this specificity role appears to have been adopted by Ste50p through its C-terminal RA domain. The RA domain of Ste50p is absolutely required to ensure proper function of the three MAPK pathways in yeast. The Ste50-RA domain apparently does not bind Ras; rather it has been found to bind the related membrane-anchored Rho small GTPase family member Cdc42p (Tatebayashi *et al.*, 2006; Truckses *et al.*, 2006), as well as a transmembrane protein, Opy2p (Wu *et al.*, 2006). Binding of these proteins with the Ste50p RA domain appears to direct Ste11p signaling in specific pathways: Opy2p in the HOG pathway (Tatebayashi *et al.*, 2006; Wu *et al.*, 2006) and Cdc42p in the pseudohyphal growth pathway (Truckses *et al.*, 2006). Pathway regulation by the Ste50p RA domain via interactions with various protein partners was found to facilitate Ste11p membrane localization, where it can be phosphorylated and activated by the PAK Ste20p. Detailed analysis of Ste50p and Opy2p interaction showed that specific peptide motifs in the disordered cytoplasmic tail of Opy2p interact with certain Ste50p RA domain residues to specifically regulate HOG signaling (Ekiel *et al.*, 2009; Yamamoto *et al.*, 2010). Interestingly, Opy2p is not required for pheromone response, as yeast cells deleted for *OPY2* show normal pheromone response (Wu *et al.*, 2006).

RA domains have been identified in many other organisms, including humans. Structurally, RA domains adopt a ubiquitin fold and are capable of interacting with a wide spectrum of partners, including the Ras small GTPase, the Raf serine/threonine protein kinase, PI3K families of lipid kinases, the Ral guanine nucleotide dissociation stimulator (RalGDS), and RASSF tumor suppressor family members (Morrison *et al.*, 1988; Rodriguez-Viciana *et al.*, 1994; Bhattacharya *et al.*, 2002; Sakai *et al.*, 2015). NMR solution structure analysis of the Ste50p RA domain indicated that it lacks the two canonical N-terminal beta-sheets required for Ras interaction, and this region is rather more unstructured (Kiel and Serrano, 2006; Ekiel *et al.*, 2009). Thus, the Ste50p RA domain defines a subfamily within the ubiquitin-like superfamily and exhibits the potential to bind partners other than Ras-like small GTPases (Harjes *et al.*, 2006; Tong *et al.*, 2007). Although it is established that the RA domain is necessary for Ste50p function in regulating the pheromone response pathway (mating), the molecular role of Ste50p function in this pathway remains unclear; specifically, whether the Ste50p RA domain is connected to the pheromone response pathway is unknown.

In this study, we have genetically probed the functioning of the RA domain of this Ste50p adaptor molecule shared by multiple MAPK pathways in yeast and analyzed how mutations affect signaling specificity. Most interestingly, mutants that are specifically defective in pheromone response provide new evidence that the Ste50-RA domain utilizes different residues to play vital roles in connecting the function of the Ste50 adaptor protein to ensure MAPK pathway signaling specificity.

RESULTS

Ste50-RA domain mutant libraries

The Ste50 adaptor protein is a 346–amino acid residue protein consisting of an N-terminal SAM and a C-terminal RA domain connected by a linker region (Figure 2A). The RA domain consists of 93 amino acids, spanning residues 235–327 (Schultz *et al.*, 1998; Kiel and Serrano, 2006; Letunic *et al.*, 2009). We randomly mutagenized (as described in *Materials and Methods*) between residues 147 and 346 spanning the RA domain to introduce point mutations generating phenotypic changes. Three libraries were built under different PCR conditions to maximize the number of events causing a few (1–3) amino acid changes per clone. The resulting libraries, consisting in total of ~72,000 primary in vivo recombination (IVR) transformants, were subjected to phenotypic screening analysis.

Screening the mutant libraries revealed four distinct phenotypes

If the Ste50-RA domain functions differently in the pheromone response pathway and the HOG pathway, one would expect that the differential RA domain functions should be genetically separable. To delineate the amino acids in the RA domain that are important for distinctive signaling properties, we performed an extensive

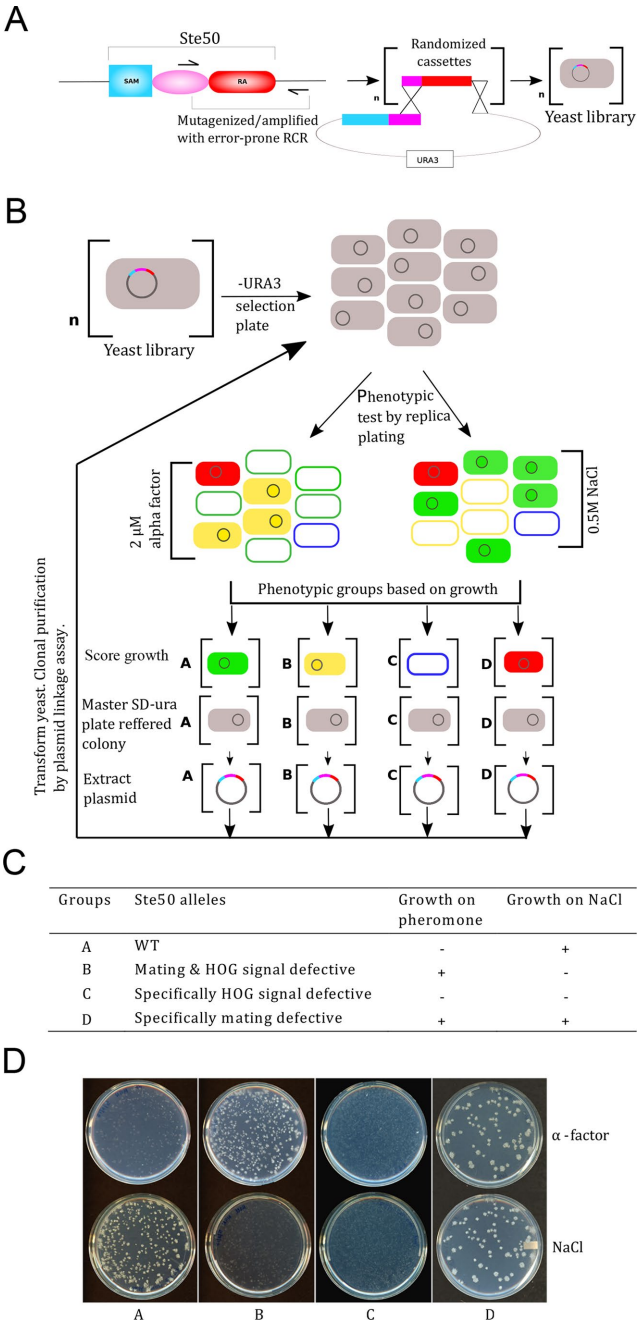

FIGURE 2: Ste50-RA domain mutant library construction and screening. (A) Random mutagenesis of Ste50-RA domain with error-prone PCR and homologous recombination in yeast was used to create the mutant libraries. (B) Library was plated on SD-ura and replicated onto selective media containing 2 μM α-factor or 0.5 M NaCl. Phenotypes were scored on both plates and grouped according to their growth patterns by comparing the plates. Library clones conferring a growth phenotype: WT green, specifically pheromone signal–defective red, specifically HOG signal–defective blue, defective in both pheromone and HOG signaling yellow. Colored filled and hollow shapes represent growth and no growth of the corresponding phenotypes, respectively (same color codes). Plasmids were extracted from colonies of each phenotypic group by referring back to the master SD-ura plates. Rescued plasmids were reintroduced into yeast to recapitulate the originally observed phenotypes (plasmid linkage assay). (C) All four expected possible phenotypes, grouped as A, B, C, and D. Growth (+) and no growth (–). (D) Phenotypes of the representative candidates obtained from the library screens.

phenotypic screen (see *Materials and Methods* and Figure 2B) for mutants in the Ste50-RA domain. We studied the ability of these mutants to show specific phenotypes. Using growth/no-growth screening conditions under pheromone and osmotic stress (see *Materials and Methods*), we anticipated four possible phenotypic combinations among the two chosen MAPK pathways (Figure 2C): 1) wild type (WT)—no growth in the presence of pheromone, normal growth under hyperosmolar stress; 2) mutants specifically defective in pheromone response—pheromone-resistant growth, hyperosmolar stress–resistant growth; 3) mutants specifically defective in HOG pathway—no growth in the presence of pheromone, hyperosmolar stress–sensitive; 4) mutants that are defective in both pathways—pheromone-resistant growth, hyperosmolar stress–sensitive. We identified all of the four above-mentioned expected phenotypes from the screens (Figure 2D). In total, 90,000 colonies were screened (equivalent to ~1.25× the combined mutant libraries) and the candidates obtained were put through further confirmations by rigorous plasmid linkage assays (see *Materials and Methods*; Figure 2B). Finally, 108 clones possessing the different phenotypic properties were selected for further analysis.

Critical residues in the Ste50-RA domain specifically control pheromone and HOG signaling pathways

To identify the mutation(s) in the final 108 clones, we performed Sanger sequencing and analyzed their sequences (see *Materials and Methods*). Sequencing revealed that 57 clones had either frame-shift mutations or introduction of stop codons leading to truncated proteins. The remaining 51 mutant clones, bearing mostly 1- to 4-point mutations, fell into the four different categories, with some recurrent hits. These mutants included seven specifically pheromone signal–defective mutants (Table 1A); nine (nonredundant) specifically HOG signal-defective mutants (Table 1B); and three (nonredundant) doubly pheromone- and HOG signal–defective mutants (Table 1C). Sequencing also identified clones showing WT function-bearing point mutations, suggesting that alterations of these residues had no detectable defect in signaling in either of the MAPK pathways investigated (Supplemental Table S1). Altogether, these mutations altered 62 unique residues in the Ste50p region amplified by PCR. Within the RA domain (Figure 3, boxed), 39 residues were changed (Figure 3, red; a total of 48 different replacements were made on these residues), generating ~42% amino acid replacements; some of these changes causing specific phenotypes supported observations made in a previous study (Ekiel *et al.*, 2009). Our results suggest that the specific amino acid substitution for a particular residue could be a crucial determinant of its functionality; for example, changing H275 from histidine to proline yielded a strong specific HOG signaling–defective phenotype, while changing it to alanine caused only a weak phenotypic effect (Table 1B; Ekiel *et al.*, 2009)

Mutants showed variability in the number of amino acid subsitutions and the strength of phenotypes displayed. In the specifically pheromone response–defective class, the strongest phenotypic mutants included M_w_1 (R283G Q294L) and H3N_3 (R296G), while the triple mutants R6 (A242G N270D I289T) and G4 (K260N L300V I307K), as well as the double mutant M10N_2_2 (V288D D328V), also showed significant pheromone response defects (Table 1A). L182P L277S mutant was isolated from multiple independent specifically HOG signal–defective clones. We wanted to identify the mutations responsible for the phenotypic effects in clones with multiple mutations, so we dissected them.

Clones	Mutations	Growth on α-factor	Growth on NaCl
A. Ste50 specifically pheromone signal–defective mutants			
H3N_3	**R296G**	+++++	++++
M_w_1	**R283G Q294L**	+++++	++++
R6	A242G N270D **I289T**	++++	++++
G4	K260N L300V **I307K**	++++	++++
M10N_2_2	V288D D328V	++++	++++
H11N_2	I289V R323G	+++	++++
M1N	**I289T**	+++	+++
B. Ste50 specifically HOG signal–defective mutants			
M6_2	K149R H219Y N250I **L277S** I320M	–	–
O2-1	K223N K225E **R274S H275Y** L322F V340G	+	–
H16	L182P **L277S**	–	–
M6	H219Y **L277S** I320M	–	–
H1N_2	S154Y **H275P**	–	–
H4N_2	A271T **L277S**	–	–
H7N_2	**H275R**	–	–
H8N_2	N250S **L277S** N310S	–	–
H9N_2	V180E **L277S** K303R N335S	–	–
C. Ste50 pheromone– and HOG signal–defective mutants			
Clone 3-7	**L322S**	+++++	–
pCW2009 (Ekiel *et al.*, 2009)	**I320K**	+++++	–
M2N_2_1	K260E C290S P304S	++++	–

++++++ is 100% functional in HOG signaling and – is 100% functional in pheromone response. Mutations causative for the observed phenotypes are in bold.

TABLE 1: Ste50-RA domain desired mutants from library screens.

For the dissections, we selected clones based on their strong phenotypic traits. From the specifically pheromone response–defective group, we selected a number of clones, since we were most interested in this new class; therefore, clones R6, G4, and M_w_1 were dissected. The R6 and G4 mutants were analyzed by gBlocks DNA synthesis (Integrated DNA technology), while M_w_1 was dissected by site-directed mutagenesis (see *Materials and Methods*). Recombinant plasmids of the variants were sequence-verified and retested in pheromone and osmotic-stress assays (Table 2 and Supplemental Figure S1). For the R6 mutant, the single mutation I289T was found to be the driver mutation (Table 2 and Supplemental Figure S1A). For the G4 triple mutant, the single mutants showed only weak phenotypes, but the strong phenotype was almost fully retained by the double mutants containing the I307K mutation (Table 2 and Supplemental Figure S1B). In the case of M_w_1 (R283G Q294L), interestingly, the double mutations were critical; both single mutants appeared to be WT (Table 2 and Supplemental Figure S1C). To further investigate the complex multiple mutational phenotypic behavior, we performed transcriptional activation assays with G4 and M_w_1 mutants and their

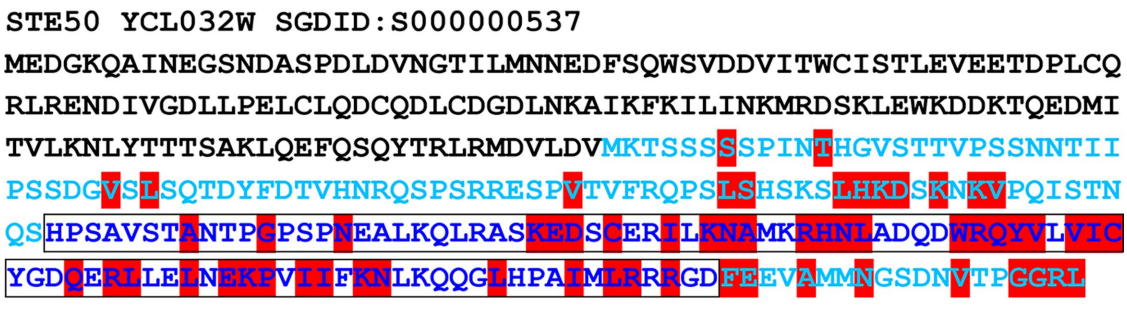

FIGURE 3: Ste50p amino acid sequence showing point mutations. The protein contains 346 amino acid residues. The RA domain spans 235–327 residues (shown boxed, dark blue; Schultz *et al.*, 1998; Kiel and Serrano, 2006; Letunic *et al.*, 2009). Error-prone mutagenic PCR has led to random changes in the region shown in light blue, which includes 62 residues that are in red.

Clones	Mutations	Growth on 2 μM α-factor	Growth on 0.5 M NaCl
R6	A242GN270DI289T	++++	+++
Dissects	A242GN270D	–	+++++
	N270D	–	+++++
	A242G	–	+++++
	I289T	++++	++++
	N270DI289T	++++	++++
	A242GI289T	++++	+++
G4	K260NL300VI307K	++++	++++
Dissects	K260N	–	+++++
	L300V	–	+++++
	I307K	–	+++++
	K260NL300V	–	+++++
	K260NI307K	++++	++++
	L300VI307K	++++	++++
M_w_1	R283G Q294L	+++++	++++
Dissects	R283G	–	++++
	Q294L	–	++++
H16	L182P L277S	–	–
Dissects	L182P	–	+++++
	L277S	–	–

TABLE 2: Mutational dissections of multiple mutations to find causal mutation(s).

mutational dissects using a FUS1-LacZ promoter–reporter system (see *Materials and Methods*; Figure 4). The double mutant M_w_1 (R283G Q294L) showed severe defect, only ~14% of the WT pheromone response. Interestingly, the dissected single mutation could not recapitulate the transcritional output of the double mutant; R283G and Q294L showed almost 80% and 39% of the WT pheromone response, respectively, where Q294L appears as the driver mutation. For the triple mutant G4 (K260N L300V I307K), all three mutations are needed for the strong pheromone response defect (Figure 4), although I307K seems to be the mutation with the greatest effect.

In addition, the HOG specific double mutant L182P L277S was subjected to site-directed mutagenesis to identify the driver mutation(s); the single mutation L277S was found to cause the observed phenotypic effects (Table 2 and Supplemental Figure S1D). The other multiple-point mutants causing strong phenotypes with defects specific to HOG signaling include at least one mutation each at positions R274, H275, and L277, as seen here and previously (Ekiel *et al.*, 2009); these positions were predicted to harbor the driver mutation in these cases (Table 1B).

Residues specifically involved in the pheromone response or the HOG signaling pathway have distinct structural localizations within the Ste50-RA domain

We have generated three groups of Ste50-RA domain mutants displaying different MAPK signaling defects. To find how these mutant residues are differentially controlling the MAPK activities, we mapped the residues onto the solution structure (Ekiel *et al.*, 2009)

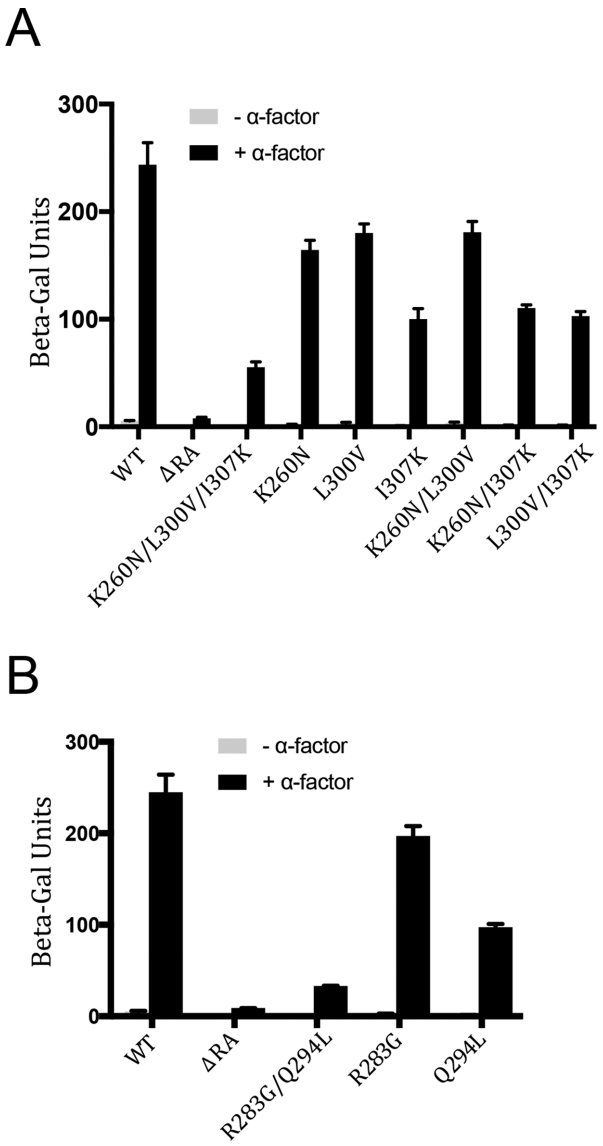

FIGURE 4: Transcriptional activation of Ste50-RA domain mutants. Yeast strains Δ*(ste50, FUS1-LacZ)* harboring Ste50-RA domain mutant G4 (K260N/L300V/I307K) and its mutational dissected derivatives (A) or mutant M_w_1 (R283G/Q294L) and its mutational dissected derivatives (B) were assayed for their ability to activate the pheromone response pathway using a FUS1-LacZ promoter-reporter. $n = 5$. Bar represents standard deviation. Beta-Gal = β-galactosidase.

of the folded RA domain (residues 251–327). The mapping showed clear structural clustering of the residues according to their phenotypic traits (Figure 5, A and B). The structural clusters responsible for controlling specific pheromone response and HOG signals reside at a distance from each other on opposite sides of the RA domain structure. Also, residues affecting both pathways are located between those pathway-specific clusters.

According to functional data for single mutants and dissected-out multiple mutants (Tables 1A and 2; Figure 4), five residues from the pheromone signaling group are R283, I289, Q294, R296, and I307. These belong mainly to the β-sheet and face away from the α1-helix and more toward the α2-helix of this peculiar RA-domain fold (Ekiel *et al.*, 2009). Among these residues, R283, Q294, R296,

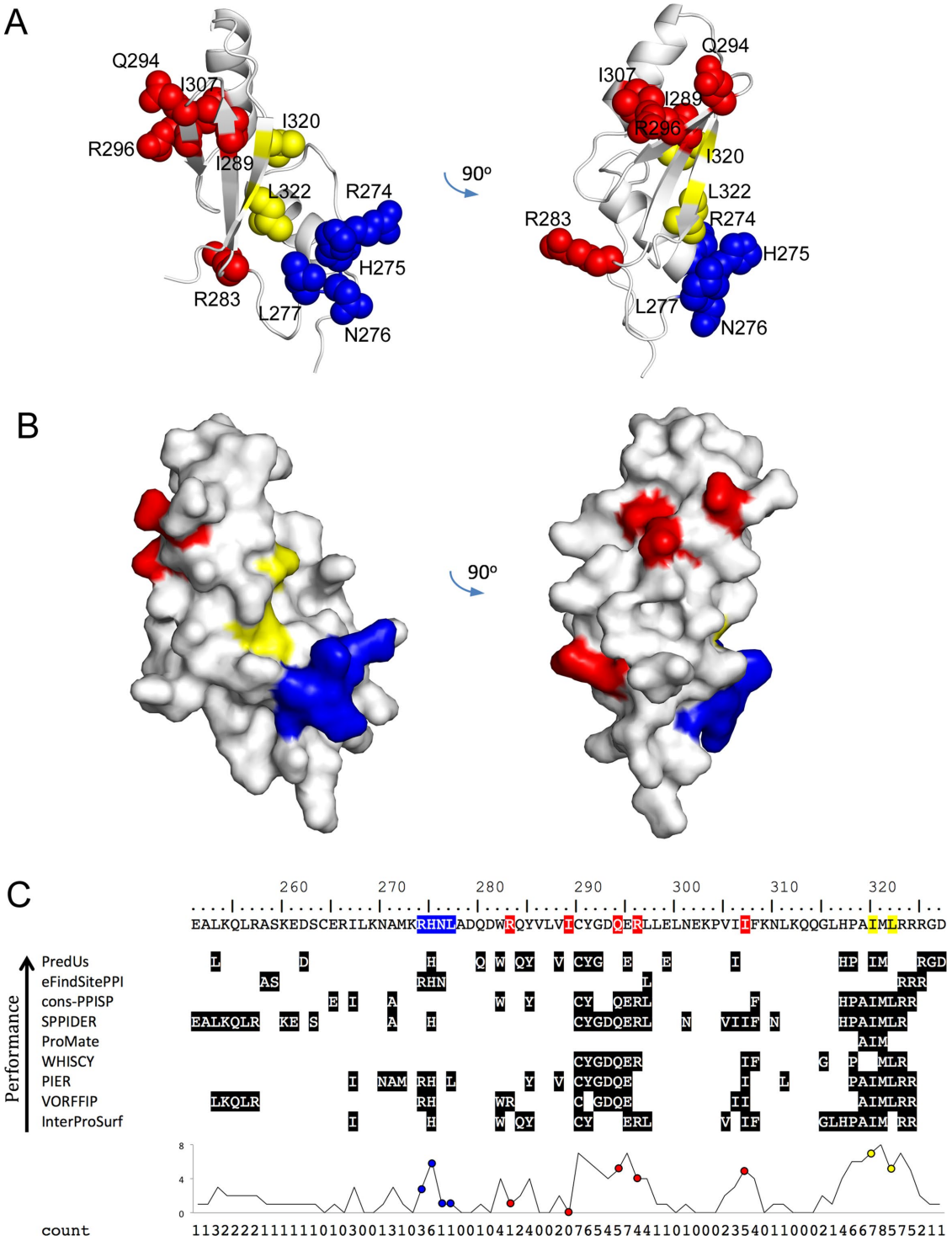

FIGURE 5: Structural clustering of Ste50-RA domain residues according to their functional phenotypes. Residues affecting the pheromone, hyperosmolar signaling, or both pathways are colored in red, blue, or yellow, respectively, and are represented as atomic spheres (A) and the molecular surface (B) of the NMR structure of the Ste50-RA domain (Ekiel *et al.*, 2009). The pathway-specific cluster residues are located at a distance from each other on opposite sides of the domain structure, and residues affecting both pathways are located between those pathway-specific clusters. (C) Structural bioinformatics metaprediction based on nine different algorithms (see *Materials and Methods*) showing the propensity of Ste50-RA domain residues to engage in protein–protein interactions. Color-coding of functional residues is as in panels A and B.

and I307 are exposed at the protein surface and, with the exception of R283, are also predicted by a structural bioinformatics metaprediction approach to have a high propensity to engage in protein–protein interactions (Figure 5C). Residue R283 is also the most structurally isolated from this group. Interestingly, R283G had only a marginal effect in the transcriptional activation assay (Figure 4),

but it consistently showed a synergistic effect when combined with the Q294L by all assays (Table 2, Figure 4, and Supplemental Figure S1C). Two computational methods employed to predict stability changes upon mutations (Supplemental Table S2) indicated that I289 mutations could lead to moderate destabilization of the Ste50-RA fold, suggesting localized conformational changes and not unfolding or significant misfolding of the domain as a result of conservative mutations of this buried residue. This is supported by the fact that the I289T mutant is functional in the HOG pathway. It is significant that the buried residue I289 is located directly underneath the surface-exposed residues belonging to the pheromone signaling cluster, emphasizing its structural role in supporting the shape of the putative protein–protein interface required for pheromone signaling.

Localized at the C-terminal end of the α1-helix and away from the pheromone signaling-associated cluster is another group of residues that, in Tables 1B and 2 and in a previous study (Ekiel *et al.*, 2009), have been shown to affect the HOG signaling pathway specifically: R274, H275, N276, and L277. These residues are surface-exposed and their mutations are predicted to be very well tolerated structurally, especially in the cases of the former three, while a minor destabilizing effect is predicted for the L277S mutant relative to the WT (Supplemental Table S2). Interestingly, residues N276 and L277 are predicted not to have a high propensity to participate in interactions with other proteins (Figure 5C).

Based on the single point–mutation data in Table 1C, residues I320 and L322 emerge as engaged in both pathways. These two residues are located on the structure of the RA domain in an area that bridges the abovementioned pathway-specific distinct clusters (Figure 5, A and B). Like the residues implicated specifically in pheromone signaling, these functionally nonspecific residues belong to the domain's β-sheet but face toward the α1-helix, where the HOG pathway–specific cluster is located. These residues also belong to regions predicted to represent potential protein–protein interaction sites (Figure 5C).

To further delineate the structural boundaries of these functional clusters, we have probed several other residues by site-directed mutagenesis based on structural analysis. None of these single mutations alone seems to have significant phenotypic effects (Supplemental Table S3), with minor defects observed only for I306E and A319E in the pheromone signaling. These additional targeted mutagenesis data may indicate relatively weak contributions from residues at these positions, which nevertheless may be amplified by combinations of several mutations as seen earlier, leading to possible expansions of the mapped functional–structural clusters. Further functional and structural work is needed to more accurately define the boundaries of these clusters.

To investigate how Ste50-RA domain functional interfaces relate to the canonical interaction mode of the RA domain with small GTPases, we overlaid the structure of the Ste50-RA domain on the RalGDS RA domain bound to the Ras small GTPase (Huang *et al.*, 1998; Supplemental Figure S2). Interestingly, the surface reponsible for the specific pheromone signaling on the Ste50-RA domain was not located near the small GTPase interaction site but rather positioned completely opposite in the structure, suggesting the possibility of binding partners for pheromone signaling that are not small GTPases.

Specifically pheromone response–defective clones show strong quantitative growth phenotypes

We focused on the strong and structurally interesting R283G Q294L and R296G mutants belonging to the pheromone response–defective class. For a quantitative assessment of the mutants' growth properties compared with those of the controls, mutants were tested in parallel by both liquid and solid growth assays. As expected, the WT Ste50–bearing strains showed severe growth retardation due to cell cycle arrest in the quantitative liquid growth assay. In contrast, the RA null mutant was clearly defective in pheromone-induced cell cycle arrest (Figure 6A) with ~4.5× more pheromone-resistant growth than in the WT. Mutants R283G Q294L and R296G had a growth pattern similar to that of Ste50ΔRA, confirming the strong pheromone-response defects of these mutants. Parallel growth assays on hyperosmolar media confirmed Ste50ΔRA to have severe growth defects while the WT could withstand the hyperosmolar stress and grow ~3× more (Figure 6B). Similarly, mutants R296G and R283G Q294L had normal growth patterns under hyperosmolar stress, as they paralleled the WT, confirming their specific pheromone-response defects (Figure 6B). Weaker alleles of specifically pheromone response–defective mutants had comparatively lower pheromone resistance growth while keeping their HOG response normal (Figure S3).

We also assessed the phenotypic growth properties for the above mutants under the same pheromone and hyperosmolar conditions by spot assays on test plates. The results for the spot assay corroborated the liquid culture assays showing growth for R283G Q294L and R296G on pheromone (Figure 6C), while both mutant strains retained their ability to grow on hyperosmolar stress (Figure 6D). Together, our results suggest that the Ste50-RA domain contains residues that are specifically required for pheromone response signaling.

Further, we tested specifically HOG signal–defective mutants, S154Y H275P, H275R, and L277S, as well as mutants that are defective in both pathways, L322S and I320K, by spot assay on test plates (see *Materials and Methods*; Supplemental Figure S4, A and B). S154Y H275P and L277S showed WT phenotype on pheromone but were unable to withstand hyperosmolar stress. On the other hand, L322S and I320K showed defective response phenotypes under both conditions.

Ste50-RA domain mutants specifically defective in pheromone response are severely defective in shmoo formation

Because prior work showed that the adaptor protein Ste50 with deleted regions confers reduced mating ability (Rad *et al.*, 1992), we speculated that the severe loss of pheromone response observed in our mutants might also have compromised some biological functions, causing morphological effects.

Differential interference contrast (DIC) microscopy studies with WT and R283G Q294L-bearing strains showed no apparent morphological differences without pheromone treatment, but gross morphological differences were observed when cells were treated with pheromone. We stimulated cells with pheromone and monitored them over a time course (see *Materials and Methods*). After as little as 1 h of stimulation, cells with WT Ste50 started to show morphological changes generating readily detectable pointed polarized structures called shmoos (Figure 7A1). Under similar conditions, the pheromone response–defective mutant R283G Q294L failed to form polarized structures and retained its unstimulated morphology (Figure 7B1). The morphological differences were more pronounced at 2 h of pheromone stimulation; R283G Q294L failed to form shmoos, while almost ~60% of the WT cells showed distinct shmoos (Figure 7, A2, B2, and D). The percentage of shmoo formation increased with time (Figure 7A3) and reached ~87% for the WT at 4 h; in contrast, R283G Q294L showed shmoos on an average of only ~10% of cells (almost sixfold < WT) (Figure 7, A4, B4, and D), providing evidence that residues 294 and 283 are

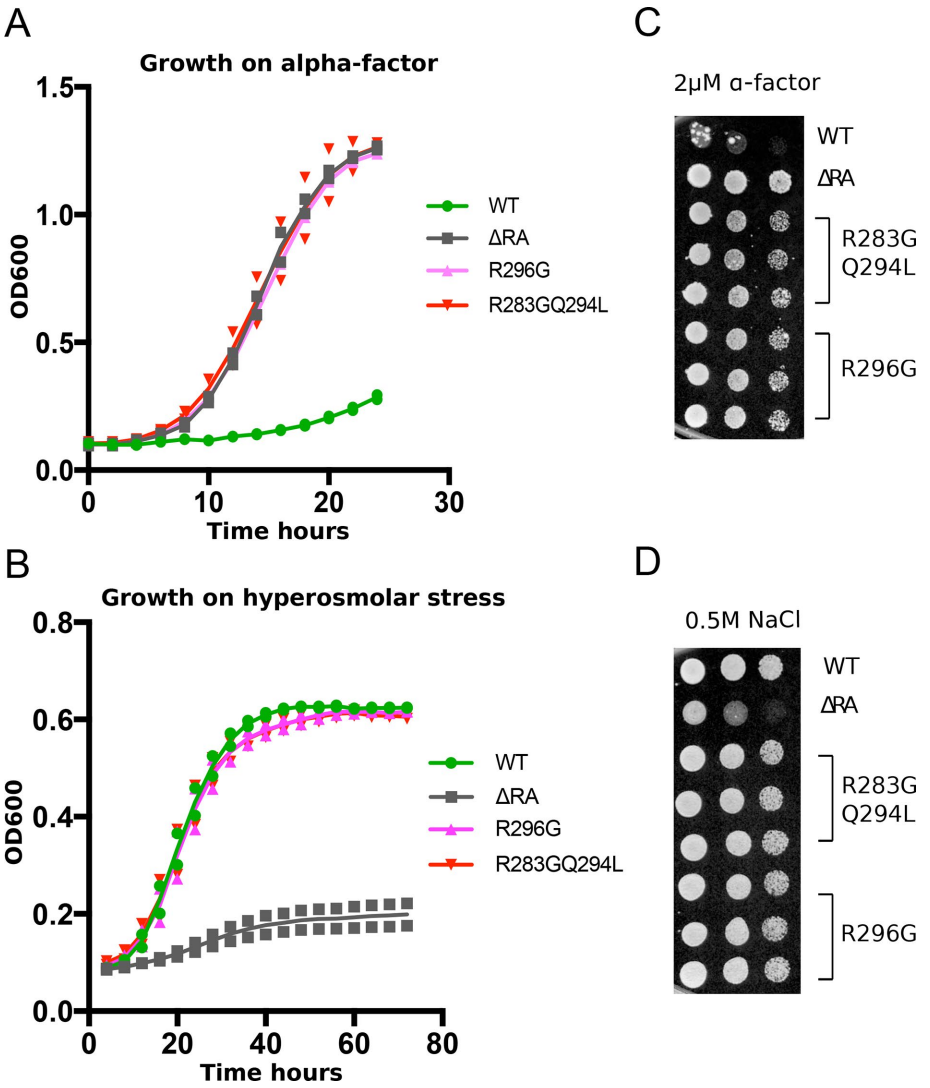

FIGURE 6: Growth characterization of Ste50-RA domain mutants specifically defective in pheromone response, showing growth in both alpha factor and hyperosmolar stress. (A, B) Growth curves for ste50 RA domain mutants. Yeast strain YCW1886 transformed with Ste50-RA domain mutants indicated or with WT or RA domain deletion constructs at OD_{600} of ~0.1 was stimulated with either 2 μM α-factor for 24 h (A) or 0.5 M NaCl for 72 h and OD measured at 10- and 15-min intervals by a TECAN machine on SD-ura selection media (B) (*Materials and Methods*) for pheromone response and hyperosmolar stress, respectively. Figures represent two trials. (C, D) Growth assay on solid media for the clones indicated of serial dilutions on SD-ura with 2 μM α-factor or 0.5 M NaCl plates scored after 2 d.

critically involved in the polarized-growth aspect of pheromone signaling.

To reinforce our finding that lack of shmooing is a feature of the specifically pheromone response–defective mutants, we also examined the shmoo-forming ability of the specifically HOG signal–defective mutant L277S. The shmoo formation of the L277S mutant showed no significant difference from the WT at 1, 2, 3, or 4 h of pheromone stimulation (Figure 7, C1–C4 and D]. Thus, in support of our growth assays, the shmoo assay also showed a severe defect in the specifically pheromone response–defective mutant R283G Q294L, while the HOG signal–defective mutant L277S showed no impairment. To determine whether the shmoo–forming ability was due to the differential expression of these alleles, we performed expression analysis of GFP-tagged mutants and WT Ste50p by immunoblotting. Our results show that the levels of protein expression of these ste50 alleles relative to the WT were unchanged (Figure 7E).

RA domain residues responsible for specific pheromone response are needed for shmoo-tip localization of Ste50p

Our microscopic studies established that mutant R283G Q294L has a grossly reduced ability to form shmoos. To examine the cellular localization of this class of mutants compared with that of WT Ste50p, we used fluorescent GFP-tagged Ste50-WT, R283G Q294L, and L277S to study their localizations (see *Materials and Methods*). Yeast cells were transformed with these fusion constructs and were verified for Ste50p functionality by testing pheromone-responsive cell cycle arrest (Supplemental Figure S5). Previously, studies have shown Ste50p to be mainly cytoplasmic (Huh *et al.*, 2003) with a fraction in the mitochondria (CYCLoPs—collections of yeast cells and localization patterns). We undertook a detailed study of Ste50p localization by cellular imaging, both in the absence and in the presence of pheromone. In the absence of pheromone, we observed WT Ste50p to be mainly cytoplasmic, confirming the previously reported observation. However, we observed that Ste50-GFP accumulated in more than 80% of cells at the shmoo tip within 1 h of pheromone stimulation (Figure 8, A1 and D). The accumulation appeared punctate and visually quite different from the master regulator of polarization, Cdc42p (Smith *et al.*, 2013). Increased accumulation was observed with the growth of the shmoo structure (Figure 8, A2–A4), and in the population level the number of shmoos with accumulation peaked around 2 h (Figure 8D).

To explore the cellular localization of the R283G Q294L mutant cells when treated with pheromone, we examined the behavior of the mutant GFP fusion protein under the same conditions and also examined the L277S–GFP fusion as a reference. Microscopic studies revealed that under pheromone treatment and over the course of 4 h, R283G Q294L not only formed markedly reduced shmoos (as discussed above) but also failed to accumulate Ste50–GFP signal at the tips that did form (Figure 8, B1–B4). Up to 2 h of pheromone stimulation, generally no observable shmoos or GFP signal accumulation were detected for R283G Q294L (Figure 8B2). Longer pheromone stimulation showed a few shmoos for R283G Q294L with barely any accumulations at the tip. Therefore, even in the presence of shmoo structures, R283G Q294L failed to accumulate Ste50–GFP at the shmoo tip, suggesting that residues 283 and 294 are required for shmoo-tip localization of Ste50. In contrast, mutant L277S–GFP accumulated at the shmoo tip like the WT (Figure 8, C1–C4). Therefore, Ste50 shmoo-tip

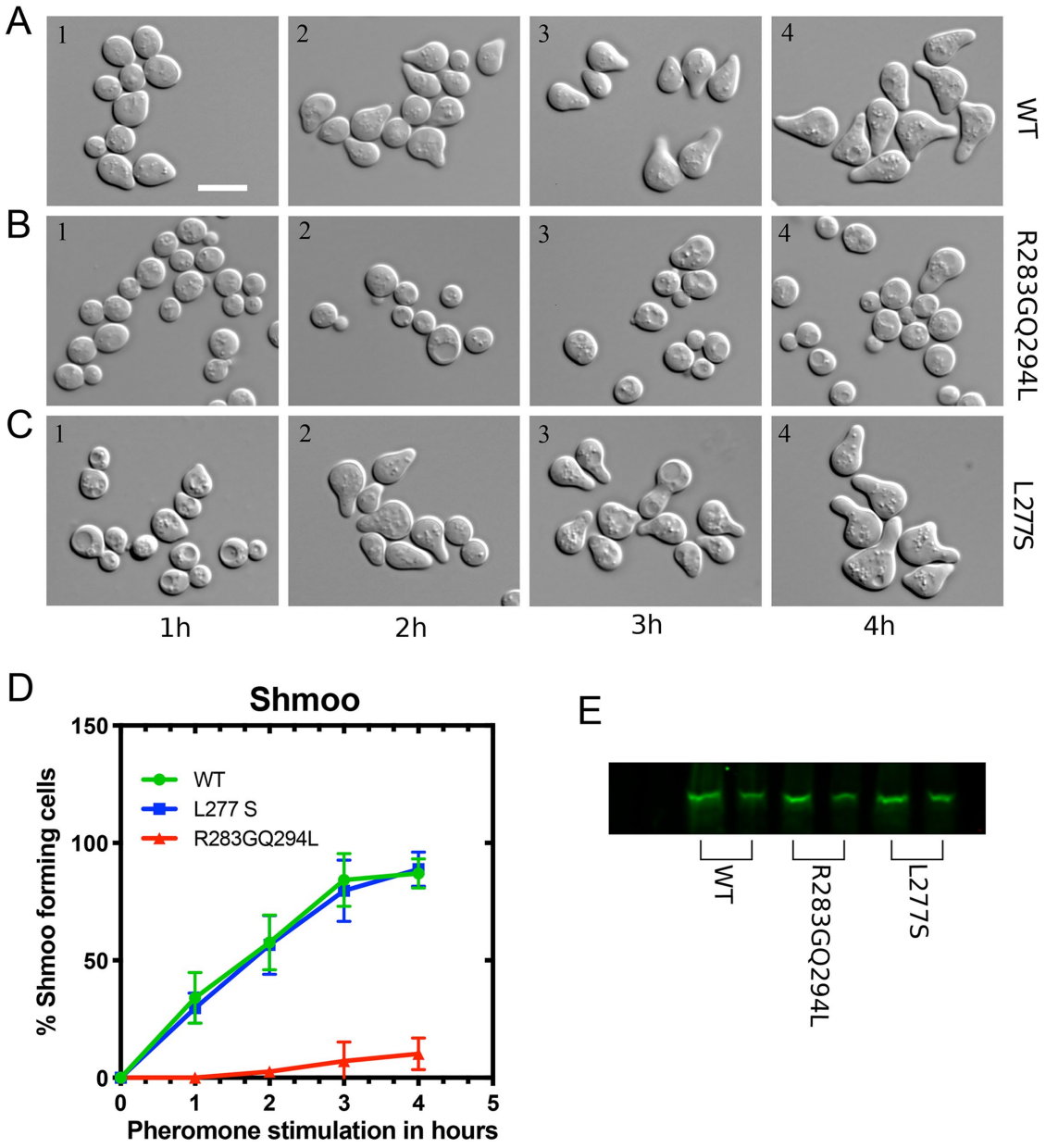

FIGURE 7: Residues 283 and 294 are critically required for shmoo formation. (A–C) Yeast cells bearing GFP-tagged WT, mutant R283G Q294L and L277S Ste50 were stimulated with 2 μM α-factor and samples collected at 1, 2, 3, and 4 h. Cells were morphologically examined under the microscope. (D) Quantitative and time-course analysis of the shmoo formation ability of Ste50p in response to pheromone as described in *Materials and Methods*. Standard deviations were calculated from five independent experiments of at least 200 cells at each time point. (E) Western blot analysis of WT Ste50p and mutants as indicated and described in *Materials and Methods*. For each Ste50 allele, lanes represent 200 and 150 μg of proteins. Bar represents 10 μm.

accumulation was unaffected by the mutation at position 277 that influences osmotic response.

DISCUSSION

Signaling pathways that share common components require mechanisms to ensure specificity of information transfer, and this specificity is often provided by adaptor molecules. Key features of such adaptors include domains (for example SH2, SH3) containing protein-binding modules that orchestrate specific protein–protein interactions (PPIs) generating larger signaling complexes; examples of such adaptors include Grb2, MYD88, and SHC1. In several yeast MAPK pathways, the SAM domain of the adaptor protein Ste50 connects to the SAM domain of a common MAPKKK termed Ste11 (Jansen *et al.*, 2001), which is a homologue of mammalian MEKKs; all are situated at the same level as Raf in their corresponding pathways. As well, the Ste50 protein contains an RA domain that controls the specificity of Ste11 signaling (Truckses *et al.*, 2006; Wu *et al.*, 2006). We previously uncovered a role of the Ste50-RA domain specifically directing signaling through the HOG pathway; the present study builds on these findings by identifying a role for the Ste50-RA domain in pheromone signaling and establishing the region required for interaction in the pheromone-response pathway. This work shows that the RA domain

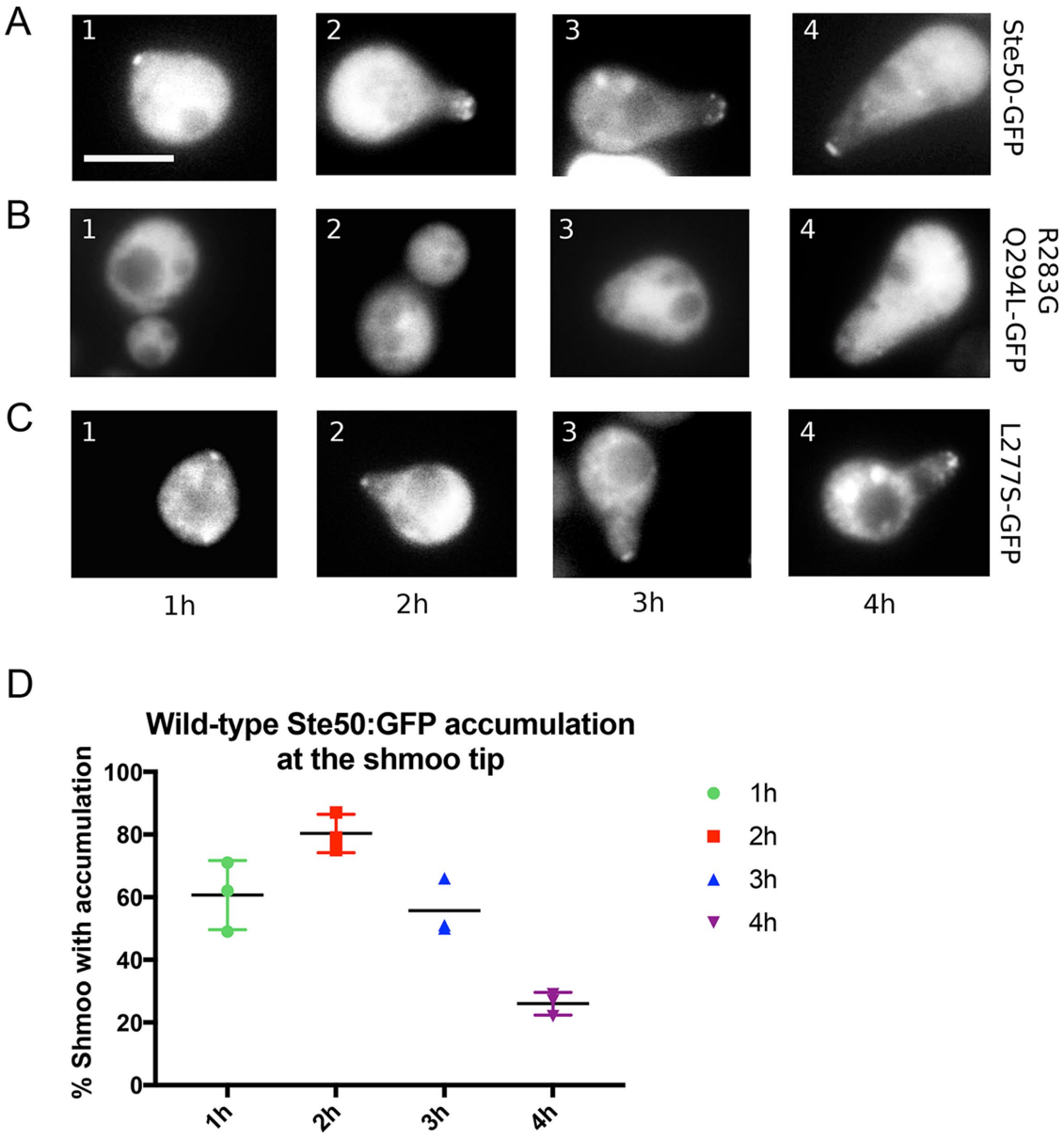

FIGURE 8: Ste50-GFP localization profile. Yeast strains expressing either WT (A), the R283GQ294L (B), or the L277S (C) RA domain mutant Ste50-GFP fusion proteins were studied microscopically to determine cellular GFP protein localization after pheromone treatment for the indicated time. WT or L277S Ste50-GFP protein localizes to the shmoo tip within 1 h of pheromone treatment (A1, C1, and D) and shows increased localization with time (A2–4, C2–4, and D). The RA domain mutant R283G Q294L shows no shmoo up to 2 h (B1 and B2) and fails to localize to the shmoo tip (B3 and B4). Results of three independent experiments at each time point. At least 100 shmoos were analyzed for shmoo accumulations, D. Bar, 5 μm.

of Ste50p uses distinct surfaces to connect specifically either to the mating-pheromone pathway or to the HOG-signaling pathway.

We randomly mutagenized the Ste50-RA domain by error-prone PCR, screened for mutants with specific MAPK-signaling phenotypes, and obtained several classes (Table 1). Among them, the class I mutants generated cells that specifically showed pheromone response–defective signaling; these cells were blocked in undergoing pheromone-dependent cell cycle arrest but remained functional in response to hyperosmolar stress. We found that the functionally important residues that are specifically involved in the pheromone response pathway (R283, I289, Q294, R296, and I307) are distinct from the residues that are involved in the HOG signaling pathway (R274, H275, N276, and L277; Tables 1 and 2). Mapping these residues onto the three-dimensional RA-domain NMR structure showed that they clustered around distinct patches (Figure 5). Residues that affected both pathways (I320 and L322) were found to be located between these two pathway-specific clusters. This clustering suggests distinct epitopes on the protein surface that may be required for interaction with partner proteins (Kiel and Serrano, 2006). Although the RA domain has a noncanonical ubiquitin fold (Ekiel *et al.*, 2009), the topology of the core still resembles the canonical ubiquitin fold, with three β-sheets and two α-helices. The patches identified in this study belong to the stable, well-folded core of the domain-encompassing amino acids 262–326 (Ekiel *et al.*, 2009). Structurally, the specifically pheromone response–defective residues belong to the β-sheet and are facing

away from the α1-helix where the specifically HOG signal–defective residues are positioned (Figure 5A), showing that these binding epitopes are on different secondary structure elements that provide different interfaces and interaction modes. A computational analysis further indicated that mutations introduced in these surface patches maintain this well-folded structure (Supplemental Table S2), suggesting that the associated phenotypic effects observed in this study were not a result of major conformational changes. The data presented here identify the structural basis of the Ste50p RA domain that differentially connects to the different MAPK pathways and potentially modulates signaling specificity.

Interestingly, we found that in two cases more than one mutation was required to bring out the desired phenotypic effect(s)—for example, R283G Q294L and K260N L300V I307K, where pheromone stimulation caused a stronger phenotypic response with the combined mutations than with the dissected component ones (Table 2). It seems that simultaneous modification of various residues may have coherently amplified individually weak structural and dynamic perturbations into stronger effects (Tripathi *et al.*, 2016).

We established by GFP tagging and live cell imaging that the WT Ste50-GFP accumulates at the shmoo tip upon pheromone stimulation, while the specifically pheromone response–defective mutants failed to localize. Generally, mutations affecting protein localization indicate loss of a transient interaction and are identified as loss-of-function kinds (Yates and Sternberg, 2013). In the WT, this accumulation at the shmoo tip strengthens with time and is punctate in nature. Because this accumulation is at the growing shmoo tip, Ste50p may be a member of the polarization complex. We carefully examined whether there is Ste50 accumulation at the young bud tip, since this was found in the case of Cdc42p (Smith *et al.*, 2013; Okada *et al.*, 2017), which is a core member of the polarization patch. We were unable to find such bud accumulation of Ste50p. Proteins unique to bud or shmoo tips have been suggested before (Narayanaswamy *et al.*, 2008). We speculate that the shmoo-tip accumulation of Ste50p could define a specific pheromone-dependent polarization module, resulting from a complex formed between Ste50p and other protein(s) unique to pheromone response. This was supported by the fact that the specifically pheromone response–defective mutants found here showed gross inability to form shmoos and failed to accumulate at the shmoo tip, but were budding normally. This was also reinforced by the fact that the specific HOG signal–defective class was WT-like with regard to shmoo accumulation. These combined results suggest that these residues are critical for pheromone-specific response, and mutating these residues may have caused loss of partner interaction(s), and hence lack of complex formation with Ste50p and localization at the pheromone-induced polarized structure—the shmoo tip.

The C-terminal RA domain of Ste50 appears to have a function in the yeast MAPK pathways similar to that of the mammalian N-terminal RA domain of Raf that interacts with Ras and is required for its delivery to the membrane. Although the RA domain of Ste50 does not bind Ras, it has been shown to bind the membrane-anchored small Rho-like GTPase Cdc42 (Tatebayashi *et al.*, 2006; Truckses *et al.*, 2006) as well as the transmembrane protein Opy2p (Wu *et al.* 2006), potentially for facilitating Ste11p membrane localization where it can be phosphorylated and activated by the PAK like Ste20p. Interestingly, these two interactions are required for Ste50 function in two different MAPK pathways, Opy2p for the HOG pathway (Wu *et al.*, 2006) and Cdc42p for the filamentous-growth pathway (Truckses *et al.*, 2006). In the HOG-signaling pathway, it was shown previously that the Ste50-RA domain requires all three residues R274 H275 N276 for its specific interaction with Opy2p (Ekiel *et al.*, 2009); here we found that a single residue, H275, when changed from histidine to proline, can alone yield a strong specific HOG-signaling defect. Logically, replacement with proline instead of alanine is likely to cause a more drastic disturbance to abrogate HOG signaling. In the filamentous growth pathway, it was shown that residues I267 and L268 of the Ste50-RA domain are required for interaction with Cdc42p small GTPase (Truckses *et al.*, 2006). Based on a structural comparison of the Ste50-RA domain using as guide the RalGDS RA domain bound to the Ras small GTPase (Supplemental Figure S2), our data show that the specifically pheromone response–defective surface on the Ste50-RA domain is located on the face opposite to the canonical binding site for small GTPases. This finding implicates a possible PPI between the Ste50-RA domain and a binding partner for pheromone response that is not a small GTPase.

The PPIs for signaling pathways are usually transient (Gibson, 2009), and the interfaces are typically smaller than permanent interfaces (Perkins *et al.*, 2010). Chavali *et al.* (2010) have proposed that a protein causing various phenotypically different diseases is usually centrally located in the PPI network, because of which it is involved with multiple biological pathways. In humans, binding of the Ras association domain with effector Ras appears to act as a molecular switch controlling a large number of pathways (Wohlgemuth *et al.*, 2005). Structurally, a common feature among Ras binding domains is their ubiquitin fold and their ability to interact with different partners. In humans, RA domains have been found to interact with a variety of partners (see the *Introduction*); in yeast, previous studies found two proteins interacting with the Ste50-RA domain. Two possibilities for engagement into PPI are that 1) the RA domain may have different surfaces and interact with many interaction partners; or 2) it may have multiple partners that share the same or overlapping interfaces, allowing only one partner to bind at a time (Kim *et al.*, 2006). Based on our study here, the Ste50-RA domain shows unique structural patches for differential MAPK signaling, indicating the possibility of engaging in PPI through scenario 1. It is possible that the structurally overlapping region between the pathway-specific clusters of the Ste50-RA domain may also be a site for protein binding, as indicated by our structural metaprediction study (Figure 5C). Cooperative binding was found for Fus1 that binds both promiscuous and selective ligands in distinct conformational modes (Reményi *et al.*, 2005).

This work identifies two distinct surface regions containing pathway-specific mutations. These regions are consistent with potential binding sites for proteins involved in specific interactions for mating and osmoregulatory signaling. Although Opy2 represents the HOG-pathway interacting protein, a candidate for a pheromone-pathway protein associating through the RA domain remains to be elucidated. Suppression studies and protein–protein association assays directed by these specificity-defining mutations represent promising avenues for identifying such a protein.

Thus, the functional repertoire of Ste50 is expanding into signal discrimination using distinct structural interaction modes. Given the structurally conserved nature and repeated employment of RA domains in signaling molecules in higher eukaryotes, the implications of this work go beyond the yeast model system in terms of our understanding of the RA domain and the mechanisms of action of this versatile protein module.

MATERIALS AND METHODS

Yeast strains, plasmids, and yeast manipulations

The yeast strain used in this study was YCW1886 (*MATa ste50Δ::KanR ssk1Δ::NatR sst1::hisG FUS1-LacZ::LEU2 his3 leu2 ura3 trp1 ade2*).

The plasmids used in this study are listed in Supplemental Table S5. The *Escherichia coli* strain used in this study was MC1061 (F⁻Δ*(ara-leu)7697 [araD139]B/r* Δ*(codB-lacI)3 galK16 galE15 λ- e14-mcrA0 relA1 rpsL150(strR) spoT1 mcrB1 hsdR2*(r⁻m+) from Invitrogen. Standard manipulations of yeast strains, culture conditions, and media were as described (Dunham *et al*., 2015). Yeast transformations were carried out by the lithium acetate method (Chen *et al*., 1992). Benchling was used for the design of plasmids and primers.

Plasmid construction

Plasmid pNS101 containing an *HIS3* stuffer marker was constructed by cloning the *HIS3* marker from pCW606 as a *Sal*I fragment into the *Sal*I site of pCW463, which contains *STE50* lacking the RA domain. Mutant ste50–GFP plasmids were constructed by PCR amplification of the mutation using the pNS102 plasmids (see below) bearing the mutation(s) as templates with primers OCW551 and ONS30 to amplify the region, plus the flanking sequences on both ends for in vivo recombination (IVR) in yeast into the *Bpu*10I linearized Ste50:GFP. The desired recombinants were confirmed by DNA sequencing.

Construction of ste50 RA domain mutant libraries

Three *STE50 RA* domain libraries were constructed using different mutagenic conditions to optimize the frequency of mutations in the *RA* region by mutagenic PCR. Briefly, PCRs were performed using plasmid pCW572 as a template with primers OCW80 and OCW164 to amplify the *STE50 RA* region, plus flanking sequences on both ends for in vivo recombination (IVR) in yeast. All primers used in this study are listed in Supplemental Table S6. Three separate PCRs were carried out with Taq DNA polymerase (New England Biolab, Montreal, Canada) under the following conditions: 1× Taq DNA polymerase buffer (New England Biolab), 0.2 mM dNTP (each) mix, 0.2 μM of each primer, ~100 ng of template DNA for 30 cycles, included in each different mutagenic stress, such as 5 mM $MgCl_2$, 7 mM $MgCl_2$, 7 mM $MgCl_2$ + 0.5 mM $MnCl_2$. The PCR products were cloned into *Eco*RI- and *Sal*I-digested plasmid pNS101 by in vivo recombination in yeast (YCW1886) to generate the mutant plasmids pNS102 (pRS-*STE50*$^{1\text{-}346}$::*URA3*/AmpR) containing libraries. The IVR clones were selected on agar plates lacking uracil; clones were counted and pooled and titers were determined.

All site-directed modifications of *STE50* were performed with a site-directed mutagenesis kit (QuikChange II XL; Agilent Technologies, Montreal, Canada) according to the manufacturer's protocol. The oligonucleotides used to generate the site-directed *ste50* mutants are listed in Supplemental Table S6. Plasmids were purified from several independent *E. coli* colonies from each mutagenesis and sequenced to verify the introduction of only the correct substitution(s). Verified plasmids were then used for phenotypic characterization.

Mutant ste50 library screening

Conditions for screening mutant libraries were established using WT Ste50 (pCW267) and Ste50-RA domain–deletion (pCW463) plasmids, challenging with α-factor for pheromone response and NaCl for hyperosmolar stress. The libraries were screened by initially plating ~200 cells/plate on synthetic defined (SD) media lacking uracil. Plates were incubated for 2 d at 30°C for colonies to grow, and then replica-plated in parallel at low density onto SD-Ura plates containing 2 μM α-factor (Sigma-Aldrich, Oakville, Canada) and SD-Ura plates with 0.5 M NaCl in galactose. After 1 d of incubation for the α-factor and 2 d for NaCl at 30°C, four different phenotypes were identified, picked from the master plate, and patched separately on SD-Ura plates: 1) nongrowers on α-factor plates and growers on hyperosmotic medium plates, 2) growers on both α-factor plates and hyperosmotic medium plates, 3) nongrowers on α-factor plates and hyperosmotic medium plates, 4) growers on α-factor plates and nongrowers on hyperosmotic plates.

Plasmid rescue, plasmid linkage test, and sequencing analysis

STE50 plasmids were recovered from the selected yeast strains with desired phenotypes and used for transformation and propagation in *E. coli*. Plasmids were extracted from *E. coli*, and DNA concentrations were determined using NanoQuant Infinite Pro 200 (TECAN, Switzerland) according to the manufacturer's protocol. Plasmid DNAs were then retransformed into yeast strain YCW1886 to ensure recapitulation of the desired phenotypes. *STE50* alleles that satisfied the selection criteria were sequenced with primers OCW93 and OCW164. All sequencing reactions were performed at the McGill University Génome Québec Innovation Centre. Nucleic and amino acid sequences were analyzed with Clustal Omega, ExPASy, and Bioinformatics.org and compared with fungal genome database (http://seq.yeastgenome.org/) to identify mutations.

Mutational dissections with site-directed mutagenesis and gBlocks synthesis

Selected clones containing multiple mutations were dissected to find the driver mutation(s). This was achieved with designed gBlock DNA synthesis (IDT, Coralville, IA; Supplemental Table S1S) containing the permutation-combinations of mutation(s). The gBlocks were cloned into *Eco*RI and *Sal*I digested plasmid pNS101 by in vivo recombination in yeast (YCW1886) to introduce the dissected mutation(s). Site-directed mutagenesis using QuikChange (Agilent Technology) was also performed to dissect mutants ste50^{L182PL277S} and ste50^{R283GQ294L} to find the causal mutation(s). To dissect ste50^{R283GQ294L}, primers ONS21 and ONS22 were used to revert the mutation at residue 283; ONS23 and ONS24 to change residue 294. For ste50^{L182PL277S}, primers ONS25 and ONS26 were used to revert the mutation at residue 182; primers ONS27 and ONS28 to change residue 277. Plasmids extracted from five independent *E. coli* clones were sequence-verified and then tested on alpha-factor and hyperosmolar stress to confirm the driver mutation(s).

Growth assay

For growth on solid media analysis, overnight cultures in synthetic defined media with amino acid dropout selection were diluted to OD_{600} of 1 followed by sixfold serial dilutions in multiwell plates. Five microliters of each dilution was spotted on prewarmed agar plates with respective selections using the indicated concentrations of alpha factor and NaCl in glucose. Plates were incubated at 30°C for 2–4 d and scored for growth.

For quantitative growth in liquid media assays, yeast strain YCW1886 was transformed with *ste50* mutants and control plasmids. Three different colonies from each transformation were grown until saturation. Fresh medium was reinoculated from the saturated cultures in 1:1000 dilutions to obtain overnight cultures at the exponential growth phase. Cultures were serially diluted in a 96-well plate to obtain OD_{600} around 0.05–0.1 and treated either with 2 μM alpha factor or 0.5 M NaCl in glucose, and the OD_{600} was measured on a TECAN machine every 10 and 15 min, respectively. Alpha factor–treated cultures were measured for 24 h and NaCl-treated cultures were monitored for 72 h. Replicate OD_{600} was plotted every 4 h for analysis.

Microscopy and live-cell imaging

Before imaging, YCW1886 strains bearing *STE50* WT and mutants on plasmids were grown to saturation in selective SD-His liquid media, diluted 1:1000 in fresh media, and incubated overnight to generate mid-exponential–stage cultures the next morning. Each culture was then divided into eight tubes, half of which received 2 μM alpha factor. Cells were incubated for several time points and samples were collected and then prepared for viewing. Imaging was performed on a DM6000 epifluorescence microscope (Leica Biosystems, Wetzlar, Germany) with Velocity acquisition software (PerkinElmer, USA) using a 100× Leica Plan Fluotar (NA 1.3) lens. Both the differential interference contrast (DIC) and the fluorescein isothiocyanate (FITC) images were obtained for the pheromone- and no pheromone–treated cells. Single–time point images of live or fixed cells were collected, and ImageJ software (*v.* 1.37; National Institutes of Health) was used to process the images. For cell counting and image analysis of morphological studies, budding cells were counted as single cells and dead cells were omitted from the count. Generally, at least 200 cells were counted for each data point from three to five biological replicates.

Immunoblotting

From freshly streaked plates containing yeast strains bearing GFP fusions to either WT or mutant *STE50*, a single colony per strain was picked and cultured overnight in –His medium and then diluted 1:1000 in 50 ml media and incubated at 30°C to OD of 0.8–1.0 the next morning. Total protein was extracted by bead beating in IP150 buffer (50 mM Tris-HCl, pH 7.4, 150 mM NaCl, 2 mM $MgCl_2$, 0.1% Nonidet P-40) that had a Complete Mini protease inhibitor cocktail tablet and a Phosphatase inhibitor cocktail tablet (Roche Applied Sciences, Penzberg, Germany). Cell lysing was done by vortexing with glass beads in microcentrifuge. To avoid heating the samples, cells were disrupted for 30–60 s with 20- to 30-s pauses on ice for a total of 3 min. The lysates were centrifuged at 14,000 rpm for 10 min at 4°C in a benchtop centrifuge (Heraeus Biofuge, Cambridge, MA) to pellet the cell debris, and the cleared supernatants were transferred to fresh Eppendorf tubes. The Bradford assay was used to estimate the protein concentrations of the lysates. Samples were then boiled with SDS–PAGE sample buffer and 150 and 200 μg of proteins for each sample were applied to prepared polyacrylamide gels (4–20%). Proteins were transferred to a nitrocellulose membrane and subsequently probed with anti-GFP primary antibody 1:1000 mouse monoclonal (Abcam, Cambridge, MA) and secondary antibody 1:10,000 IRDye800 conjugated goat anti-mouse immunoglobulin G (polyclonal) from LI-COR (Lincoln, NE). Blots were visualized by an LI-COR Odyssey imaging platform (Lincoln, NE) to detect the fluorescent secondary antibody.

Structural bioinformatics

The minimized average NMR structure of the Ste50-RA domain residing in E251-D327 (Ekiel *et al.*, 2009) was used for structural bioinformatics analysis in this study. Molecular structure display, rendering, and examination were done in PyMol (Schroedinger, New York). Predictions of change in stability (folding free energy) upon mutations of the WT protein were carried out with the mCSM (Pires *et al.*, 2014) and FoldX (Guerois *et al.*, 2002) methods using default settings, as well as those implemented in ADAPT (Vivcharuk *et al.*, 2017) for FoldX stability calculations. Predictions of PPI sites were done with nine structure-based methods benchmarked against a set of known protein–protein complexes with experimentally determined crystal structures (Maheshwari and Brylinski, 2015). Predictions for probable PPI residues were based on the default score thresholds for each method or, in the absence of a recommended threshold, as follows: residues predicted by at least nine servers for SPPIDER; positive scores for WHISCY; scores greater than 10 for PIER; scores greater than 0.7 for VORFFIP. InterProSurf predictions were based on combined patch and cluster analyses. The species homologue alignment of the Ste50-RA domain from Figure S1 of Ekiel *et al.* (2009) was used as input in WHISCY.

β-Galactosidase assay

Quantitative β-galactosidase reporter assays for the pheromone response pathway were performed as described (Wu *et al.*, 1999; Tatebayashi *et al.*, 2006). YCW1886 cells bearing Ste50 WT, mutants, and control vector were grown in selective SD-Ura medium at 30°C to late exponential phase and then induced with either 2 μM α-factor for 4 h at 30°C. Beta-galactosidase activities were measured and expressed as $(OD420 \times 1000)/(OD600 \times t \times v)$, where t is in minutes and v is in milliliters (Miller, 1972).

ACKNOWLEDGMENTS

This research was supported by a Natural Sciences and Engineering Research Council (NSERC) of Canada grant (C.W.), NSERC CRC Tier 1 950-22895 (M.W.), and McGill University. We thank Brian Slaughter for sharing the WT Ste50-GFP plasmid.

REFERENCES

Bhattacharya M, Anborgh PH, Babwah AV, Dale LB, Dobransky T, Benovic JL, Feldman RD, Verdi JM, Rylett RJ, Ferguson SS (2002). β-Arrestins regulate a Ral-GDS–Ral effector pathway that mediates cytoskeletal reorganization. Nat Cell Biol 4, 547–555.

Chavali S, Barrenas F, Kanduri K, Benson M (2010). Network properties of human disease genes with pleiotropic effects. BMC Syst Biol 4, 78.

Chen D, Yang B, Kuo T (1992). One-step transformation of yeast in stationary phase. Curr Genet 21, 83–84.

Craig EA, Stevens MV, Vaillancourt RR, Camenisch TD (2008). MAP3Ks as central regulators of cell fate during development. Dev Dyn 237, 3102–3114.

Dunham MJ, Gartenberg MR, Brown GW (2015). Methods in Yeast Genetics and Genomics, Cold Spring Harbor, NY: Cold Spring Harbor Laboratory Press.

Ekiel I, Sulea T, Jansen G, Kowalik M, Minailiuc O, Cheng J, Harcus D, Cygler M, Whiteway M, Wu C (2009). Binding the atypical RA domain of Ste50p to the unfolded Opy2p cytoplasmic tail is essential for the high-osmolarity glycerol pathway. Mol Biol Cell 20, 5117–5126.

Gibson TJ (2009). Cell regulation: determined to signal discrete cooperation. Trends Biochem Sci 34, 471–482.

Guerois R, Nielsen JE, Serrano L (2002). Predicting changes in the stability of proteins and protein complexes: a study of more than 1000 mutations. J Mol Biol 320, 369–387.

Gustin MC, Albertyn J, Alexander M, Davenport K (1998). MAP kinase pathways in the yeast *Saccharomyces cerevisiae*. Microbiol Mol Biol Rev 62, 1264–1300.

Harjes E, Harjes S, Wohlgemuth S, Muller KH, Krieger E, Herrmann C, Bayer P (2006). GTP-Ras disrupts the intramolecular complex of C1 and RA domains of Nore1. Structure 14, 881–888.

Herskowitz I (1995). MAPK kinase pathways in yeast: for mating and more. Cell 80, 187–197.

Huang L, Hofer F, Martin GS, Kim SH (1998). Structural basis for the interaction of Ras with RalGDS. Nat Struct Mol Biol 5, 422.

Huh WK, Falvo JV, Gerke LC, Carroll AS, Howson RW, Weissman JS, O'shea EK (2003). Global analysis of protein localization in budding yeast. Nature 425, 686–691.

Jansen G, Bühring F, Hollenberg CP, Rad MR (2001). Mutations in the SAM domain of STE50 differentially influence the MAPK-mediated pathways for mating, filamentous growth and osmotolerance in *Saccharomyces cerevisiae*. Mol Genet Genomics 265, 102–117.

Kiel C, Serrano L (2006). The ubiquitin domain superfold: structure-based sequence alignments and characterization of binding epitopes. J Mol Biol 355, 821–844.

Kim PM, Lu LJ, Xia Y, Gerstein MB (2006). Relating three-dimensional structures to protein networks provides evolutionary insights. Science 314, 1938–1941.
Letunic I, Doerks T, Bork P (2009). SMART6, recent updates and new developments. Nucleic Acids Res 37, D229–D232.
Maheshwari S, Brylinski M (2015). Predicting protein interface residues using easily accessible on-line resources. Brief Bioinform 16, 1025–1034.
Mayer BJ (2015). The discovery of modular binding domains: building blocks of cell signalling. Nat Rev Mol Cell Biol 16, 691–698.
Miller JH (1972). Experiments in Molecular Genetics, Cold Spring Harbor, NY: Cold Spring Harbor Laboratory.
Morrison DK, Kaplan DR, Rapp U, Roberts TM (1988). Signal transduction from membrane to cytoplasm: growth factors and membrane-bound oncogene products increase Raf-1 phosphorylation and associated protein kinase activity. Proc Natl Acad Sci USA 85, 8855–8859.
Narayanaswamy R, Moradi EK, Niu W, Hart GT, Davis M, McGary KL, Ellington AD, Marcotte, EM (2008). Systematic definition of protein constituents along the major polarization axis reveals an adaptive reuse of the polarization machinery in pheromone-treated budding yeast. J Proteome Res 8, 6–19.
Okada S, Lee ME, Bi E, Park HO (2017). Probing Cdc42 polarization dynamics in budding yeast using a biosensor. Methods Enzymol 589, 171–190.
O'Rourke SM, Herskowitz I, O'Shea EK (2002). Yeast go the whole HOG for the hyperosmotic response. Trends Genet 18, 405–412.
Patterson JC, Klimenko ES, Thorner J (2010). Single-cell analysis reveals that insulation maintains signaling specificity between two yeast MAPK pathways with common components. Sci Signal 3, ra75.
Pawson T, Scott JD (1997). Signaling through scaffold, anchoring, and adaptor proteins. Science 278, 2075–2080.
Perkins JR, Diboun I, Dessailly BH, Lees JG, Orengo C (2010). Transient protein–protein interactions: structural, functional, and network properties. Structure 18, 1233–1243.
Pires DE, Ascher DB, Blundell TL (2014). mCSM: predicting the effects of mutations in proteins using graph-based signatures. Bioinformatics 30, 335–342.
Posas F, Witten EA, Satio H (1998). Requirement of STE50 for osmostress-induced activation of the STE11 mitogen-activated protein kinase kinase kinase in the high-osmolarity glycerol response pathway. Mol Cell Biol 18, 5788–5796.
Qamra R, Hubbard SR (2013). Structural basis for the interaction of the adaptor protein grb14 with activated ras. PLoS One 8, e72473.
Rad MR, Xu G, Hollenberg CP (1992). STE50, a novel gene required for activation of conjugation at an early step in mating in *Saccharomyces cerevisiae*. Mol Gen Genet 236, 145–154.
Reményi A, Good MC, Bhattacharyya RP, Lim WA (2005). The role of docking interactions in mediating signaling input, output, and discrimination in the yeast MAPK network. Mol Cell 20, 951–962.
Rodriguez-Viciana P, Warne PH, Dhand R, Vanhaesebroeck B, Gout I, Fry MJ, Waterfield MD, Downward J (1994). Phosphatidylinositol-3-OH kinase as a direct target of Ras. Nature 370, 527–532.
Sakai N, Saito Y, Fujiwara Y, Shiraki T, Imanishi Y, Koshimizu TA, Shibata K (2015). Identification of protein arginine N-methyltransferase 5 (PRMT5) as a novel interacting protein with the tumor suppressor protein RASSF1A. Biochem Biophys Res Commun 467, 778–784.
Schultz J, Milpetz F, Bork P, Ponting CP (1998). SMART, a simple modular architecture research tool: identification of signaling domains. Proc Natl Acad Sci USA 95, 5857–5864.
Smith SE, Rubinstein B, Pinto IM, Slaughter BD, Unruh JR, Li R (2013). Independence of symmetry breaking on Bem1-mediated autocatalytic activation of Cdc42. J Cell Biol 202.7, 1091–1106.
Songyang Z, Shoelson SE, Chauduri M, Gish G, Pawson T, Haser WG, King F, Roberts T, Ratnofsky S, Lechleider RJ, *et al*. (1993): SH2 domains recognize specific phosphopeptide sequences. Cell 72, 767–778
Stein EG, Ghirlando R, Hubbard SR (2003). Structural basis for dimerization of the Grb10 Src Homology 2 domain. Implications for ligand specificity. J Biol Chem 278, 13257–13264
Tatebayashi K, Yamamoto K, Tanaka K, Tomida T, Maruoka T, Kasukawa E, Saito H (2006). Adaptor functions of Cdc42, Ste50, and Sho1 in the yeast osmoregulatory HOG MAPK pathway. EMBO J 25, 3033–3044.
Tong Y, Chugha P, Hota PK, Alviani RS, Li M, Tempel W, Shen L, Park HW, Buck M (2007). Binding of Rac1, Rnd1, and RhoD to a novel Rho GTPase interaction motif destabilizes dimerization of the plexin-B1 effector domain. J Biol Chem 282, 37215–37224.
Tripathi A, Gupta K, Khare S, Jain PC, Patel S, Kumar P, Pulianmackal AJ, Aghera N, Varadarajan R (2016). Molecular determinants of mutant phenotypes, inferred from saturation mutagenesis data. Mol Biol Evol 33, 2960–2975.
Truckses DM, Bloomekatz JE, Thorner J (2006). The RA domain of Ste50 adaptor protein is required for delivery of Ste11 to the plasma membrane in the filamentous growth signaling pathway of the yeast *Saccharomyces cerevisiae*. Mol Cell Biol 26, 912–928.
Vivcharuk V, Baardsnes J, Deprez C, Sulea T, Jaramillo M, Corbeil CR, Mullick A, Magoon J, Marcil A, Durocher Y, O'Connor-McCourt MD (2017). Assisted design of antibody and protein therapeutics (ADAPT). PLoS One 12, e0181490.
Wohlgemuth S, Kiel C, Kramer A, Serrano L, Wittinghofer F, Herrmann C (2005). Recognizing and defining true Ras binding domains I: biochemical analysis. J Mol Biol 348, 741–58.
Wu C, Jansen G, Zhang J, Thomas DY, Whiteway M (2006). Adaptor protein Ste50p links the Ste11p MEKK to the HOG pathway through plasma membrane association. Genes Dev 20, 734–746.
Wu C, Leberer E, Thomas DY, Whiteway M (1999). Functional characterization of the interaction of Ste50p with Ste11p MAPKKK in *Saccharomyces cerevisiae*. Mol Biol Cell 10, 2425–2440.
Yamamoto K, Tatebayashi K, Tanaka K, Saito H (2010). Dynamic control of yeast MAP kinase network by induced association and dissociation between the Ste50 scaffold and the Opy2 membrane anchor. Mol Cell 40, 87–98.
Yates CM, Sternberg MJ (2013). The effects of non-synonymous single nucleotide polymorphisms (nsSNPs) on protein–protein interactions. J Mol Biol 425, 3949–3963.